*Khulna University Studies* Special Issue ICSTEM4IR: 855-862, 2022

ORIGINAL ARTICLE

SCIENCE & ENGINEERING



# INFERENCE OF IRREGULAR CARDIAC ACTIVITY USING NEURAL TEMPORAL PERTURBATION FIELDS

**Mainul Islam Labib, Md. Tariq Hasan, Dr. Abdullah-Al Nahid***

*Electronics and Communication Engineering Discipline, Khulna University, Khulna–9208, Bangladesh*

KUS: ICSTEM4IR-22/0153

Manuscript submitted: July 21, 2022 Accepted: September 28, 2022

**Abstract**

Early diagnosis of irregular cardiac activity through existing tools such as Electrocardiogram and greater understanding of the underlying processes is critical for saving lives. Cardiac activity originates from a deterministic dynamical system of heart with trajectories following a linear map. Irregular cardiac activity observed in arrhythmia patients adds nonlinearities to the evolution function of the dynamical system underneath. Therefore, it is of great importance to quantitatively measure this non-linearity as a biomarker for impending cardiac diseases in patients. In this work, we formulated a novel mechanism named Neural Temporal Perturbation Field where perceived nonlinearities are modeled through deep neural network with perturbated inputs. Here, we examined the nonlinear state space by modeling the volatility of outputs for slightly adjusted inputs. We discovered that volatility characteristics clearly define a decision threshold that may be employed as a biomarker in clinical practice by applying our technique to data on normal and abnormal heart activity. Our approach resulted in the greater understanding of nonlinearity and volatility of irregular cardiac activity and as a biomarker achieved comparatively better accuracy than the state-of-the-art models.

**Keywords:** Cardiac irregularity, Neural Perturbation Fields, Bayesian Networks

## Introduction

Analysis of cardiac activity from mathematical perspectives; ranging from dynamical systems approach to machine learning; is essential to understand the underlying electromechanical system to design novel biomarkers for diagnosis and treatments. Cardiac activity is defined as an observable variable of electrical activity of the heart which originates from a complex dynamical system. Electrocardiography (ECG); though one of the most available approaches for recording said cardiac activity; is not enough for inferring conclusions about the underlying system due to its propensity towards false positive diagnosis. Nevertheless, proper diagnosis of cardiac diseases is imperative since sudden and unexpected cardiac death is the leading cause of death worldwide, accounting for almost 17 million deaths every year (Chugh, 2008).

Traditional insights about cardiac activity are drawn from computational models of ECG where expert

*Corresponding author: <munnaurp17@gmail.com>
DOI: https://doi.org/10.53808/KUS.2022.ICSTEM4IR.0153-se

assumptions are placed as priors. There are existing approaches in literature where said methodology is followed. Noponen et al. used invariant trajectories of the phase space to classify irregularities in cardiac activity. They hypothesized External impacts can be distinguished from genuine system changes using statistical shape theory. External effects are described as a transformation group operating on the phase space, and variance in trajectories not explained by transformations is compensated for using principal component analysis (Noponen, 2009). Shiogai et al. used nonlinear dynamics such as; Heart Rate Variability (HRV), Respiratory Sinus Arrhythmia (RSA) and Respiratory Frequency Variability (RFV); derived from ECG as a biomarker for cardiovascular aging. They also reviewed analyses of blood flow signals recorded with laser Doppler flowmetry and related it to the current understanding of how endothelial-dependent oscillations evolve with age (Shiogai, 2010). Some authors have used Bayesian networks to tap into the probabilistic nature of cardiac activity. de Oliveira et al. used dynamic Bayesian Network framework as a tool to classify heart beats in long term ECG records. Here, they devised a two layered decision support system where first layer performs segmentation and second layer performs classification (de Oliveira, 2011). ECG fiducial point extraction using dynamic Bayesian networks; such as extended Kalman Filter (KF), Hidden Markov Model (HMM) and switching Kalman Filter (sKF); was achieved (Akhbari, 2017).

In previous works, ECG is studied as a deterministic system with certain nonlinear characteristics and as inputs to Bayesian networks for classification. While these approaches have been successful at explaining underlying dynamics, they don't explain the underlying volatility induced due to added stochastic nature in irregular activity. To address that, we have devised an approach where a Temporal Perturbation Field is defined from ECG using a neural network and then a Bayesian Network is fitted on the said Neural Temporal Perturbation Field to calculate volatility, long-range and short-range dependency parameters for both regular and irregular cardiac activity.

## Materials and Methods

### *Dataset*

In this work, electrocardiogram (ECG) recordings of 290 subjects (mean age 57.2) from the PTB Diagnostic Database are used (Bousseljot, 1995). The traditional 12 leads I ii, iii, avr, avl, avf, v1, v2, v3, v4, v5, v6), as well as the three Frank lead (vx, vy, vz) ECGs, are all measured concurrently in each record with sampling rate 1000Hz (Goldberger, 2000). We also devised a mechanism using Arduino Uno Micro-controller and AD8232 Analog to Digital Converter based ECG Module to collect single channel ECG data ourselves as shown in Figure 1. Analog data collected from ECG module are transmitted to local host server using the Arduino Uno micro-controller with a sampling rate of 400Hz. We collected cardiac activity data from 8 subjects with mean age of 21, mean weight of 71.5 and mean height of 176 cm. We deployed frequency filtering on the recorded data for three types of noise: 1. Wandering Noise (5-12 Hz) 2. Powerline Interference (<50Hz) 3. Motion Artifact (1-3 Hz)

### *Neural Field*

A field is a mathematical structure consisting of a number or tensor providing value for each realization across space and time. A neural field; according to the universal approximation theorem; is a field that is parameterized fully or in part by a neural network. Any field $f(x,t)$ is a neural field if and only if $f_\theta$ parametrized by $\theta$ is a

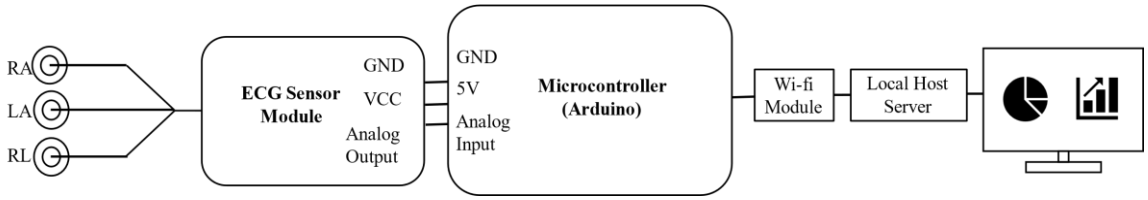


Figure 1. System Diagram of the used system in data collection.

neural network (Xie, 2021). Continuity and adaptability are by design the key characteristics of neural fields. Unlike discrete parameterizations, which scale poorly with spatial and temporal resolution, the memory required for neural fields grows with the number of parameters in the neural network. While this increase in network complexity can be hard to adjust, but it removes the problem of not knowing complexity before-hand in other continuous parametrizations such as Fourier Series. Neural fields are often designed with activation functions who have well-defined gradients allowing for optimization algorithms such as gradient descent. Especially, in the case of over-parameterization, complex signals can be regressed and optimized using neural fields (Balda, 2018).

***Neural temporal perturbation field***

In signal processing, perturbation analysis; also known as sensitivity analysis; is used to analytically quantify the deviation at a system's output that arises as a result of a known disturbance at the system's input and adversarial examples are used as perturbed version of training samples to test model performance. According to Perturbation theory, any deviation from the original output can be expressed as a power series of the perturbation parameter. In this work, a regression problem is studied using Perturbation analysis in the following manner. Given, $N$ samples $\{(x_i, y_i)\}_{i=1}^{N}$ drawn from joint probability distribution $P_{XY}$, a regression model finds the optimized parameters $\theta$ for a function $f_\theta: \mathbb{R}^M \to \mathbb{R}^M$ such that expected loss $\mathbb{E}[\mathcal{L}(f_\theta(x), y)]$ is minimized where $f_\theta$ is a neural network with arbitrary number of layers.

In this work, for $N$ samples from $\left\{\binom{x_t \; x_{t+1}}{\delta_t, \delta_{t+1}}\right\}_{t=1}^{N}$ from some distribution $P_{x_t, x_{t+1}}$ with $x_t \in \mathbb{R}^{M-1}$, our regression model finds $f_\theta: \mathbb{R}^M \to \mathbb{R}^M$ with perturbation parameter $\eta$ such that expected loss in minimized [9]. During the training process, the neural network $f_\theta$ takes $\binom{x_t}{\delta_t}$ as input where $x_t$ is the state vector at time $t$ and $\delta_t$ is the cosine similarity between $x_t$ and $x_{t+1}$. The objective of $\delta_t$ is to provide $f_\theta$ with similarity information on the state vectors' evolution such that $f_\theta: \delta_t \to \delta_{t+1}$. As for the model architecture of $f_\theta$, we chose a Multi Layered Perceptron (MLP) with activation function $g(x) = \tanh(x)$. From Figure 2-A, $f_\theta$ is trained with restrictive bounds with no regularizers such that $f_\theta$ is overfitted since our aim is not to find a generalized mapping for regression but to parametrize the evolution function through the transition probabilities from $P_{x_t, x_{t+1}}$. During the testing process; as shown in Figure 2-A; perturbation is performed on the cosine similarity between adjacent state vectors while state vectors themselves are kept same. The perturbed similarity index is defined as follows.

$$\hat{\delta}_t \sim N(\eta\delta_t, \beta_t) \tag{1}$$

where $N(.)$ is the Gaussian distribution with mean $\eta\delta_t$ and standard deviation $\beta_t$ which is defined as $\beta_t = 1 - \delta_t$. The motivation behind this formulation is to explore the tangent space of any state vector during perturbation as shown in Figure 2-B. When the perturbation parameter $\eta = 0$, $\hat{\delta}_t$ returns values closer to zero and therefore, will result in perturbation in the tangent space of that state vector. When $\eta = 1$, $\hat{\delta}_t \approx \delta_t$ and it becomes similar to the testing case. Now, the perturbation field $\Omega$ at time $t$ and perturbation realization $i$,

$$\Omega(i, t) = f_\theta \begin{pmatrix} x_t \\ \hat{\delta}_t^i \end{pmatrix}; \forall i \in I, t \in T \tag{2}$$

where $\hat{\delta}_t^i$ is the $i$-th draw from distribution defined above. Perturbation Field $\Omega \in \mathbb{R}^{T \times I \times M-1}$ is a tensor which is often intractable in volatility analysis. For mathematical comfort, we defined the flow field of $\Omega$ defined as follows.

$$\Delta(i,t) = \vec{V} \,.\, \Omega(i,t) \tag{3}$$

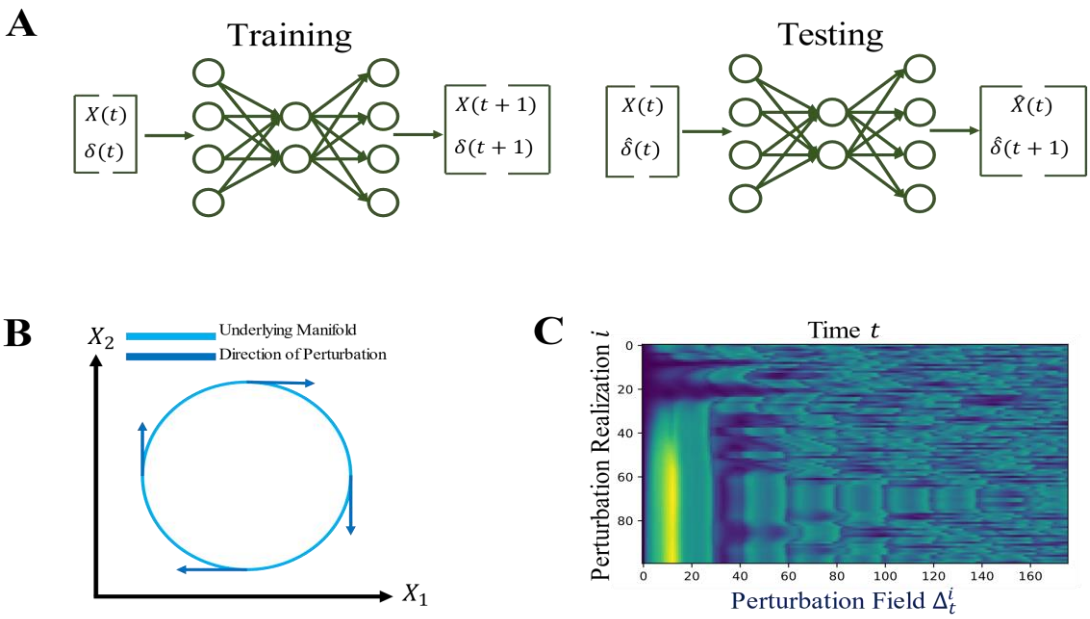


Figure 2. A. Structure of the MLP during training and Testing. $\hat{\delta}(t)$ is the perturbed cosine similarity and $\hat{X}(t)$ is output for the perturbed input. B. Direction of perturbation according to the tangent space of the underlying manifold. C. Flow of the Neural Temporal Perturbation Field for realizations $i \in I$ and times$t \in T$.

***Bayesian network on perturbation field***

Flow of the Perturbation Field $\Delta \in \mathbb{R}^{T \times I}$ has stochastic characteristics due to the probabilistic nature of $\hat{\delta}_t$ and $f_\theta$. A stochastic differential equation fitted on $\Delta$ theoretically should explain the probabilistic nature. But, since $f_\theta$ is inherently the evolution function from $x_t$ to $x_{t+1}$, $\Delta$ has also deterministic ideals. To catch both deterministic and stochastic features of $\Delta$, we define a Bayesian Network on $\Delta$ parametrized by autoregressive and volatility parameters $\sigma$.

From Figure 3-A, our proposed Bayesian Network has three nodes: $X, Y, Z$. $X$ defines the value of the flow field at time $t$ and realization $i$; therefore $X = \Delta_t^i$. $Y = \Delta_t^{i-1}$ and $Z = \Delta_{t-1}^i$ define field values at previous realization and previous time step respectively. From Figure 3-B, any value $\Delta_t^i$ in the field has a forward pass and downward pass to it. Therefore, we hypothesized that $\Delta_t^i$ can be explained as linear function of both passes while being parametrized by stochastic volatility. We define two Auto-Regressive models $AR_d(w)$ and $AR_f(w)$ of order $w$ for forward and downward passes respectively. To learn the parameters; especially $\sigma_f$ and $\sigma_d$; we employ Maximum Likelihood Estimation (MLE) scheme where random variables $X, Y$ and $Z$ are defined for $\Delta_t^i$, $\Delta_t^{i-1}$ and $\Delta_{t-1}^i$ respectively as shown in Figure 3-A. Expressions of $AR$ models for MLE estimation are defined as follows.

$$P_{X|Y}\left(\Delta_t^i \middle| \Delta_t^{i-1}, \dots, \Delta_t^{i-w}; \theta_d\right) \sim N\left(C_d + \textstyle\sum_{j=1}^{w} \phi_d^j \Delta_t^{i-j}, \sigma_d\right) \tag{4}$$

$$P_{X|Z}\left(\Delta_t^i \middle| \Delta_{t-1}^i, \dots, \Delta_{t-w}^i; \theta_f\right) \sim N\left(C_f + \textstyle\sum_{j=1}^{w} \phi_f^j \Delta_{t-j}^i, \sigma_f\right) \tag{5}$$

where $\theta_f = [C_f, \Phi_f, \sigma_f]$ and $\theta_d = [C_d, \Phi_d, \sigma_d]$. Here, forward pass and downward pass are evaluated separately to estimate $\Delta$. But since both of the passes have influence over $\Delta$, information from both probability distributions $P_{X|Y}$ and $P_{X|Z}$ have to combined into $P_{X|Y,Z}$ to infer posterior probability. (See Appendix A)

$$P_{X|Y,Z} = P_{X|Y} P_{X|Z} \tag{6}$$

Now, to find the optimum parameters, we have to maximize the log of the likelihood function $\mathcal{L}(\Theta|X)$ of seeing the data given the parameters $\Theta = [\theta_f, \theta_d]$ (see Appendix B for full derivation of the log-likelihood function)

$$\mathcal{L}(\Theta|X) = \sum_{i=w}^{|I|} \sum_{t=w}^{|T|} \left[\log P_{X|Y}\left(\Delta_t^i\right) + \log P_{X|Z}(\Delta_t^i)\right] \tag{7}$$

$$\Theta = \arg\max_{\Theta} \mathcal{L}(\Theta|X) \tag{8}$$

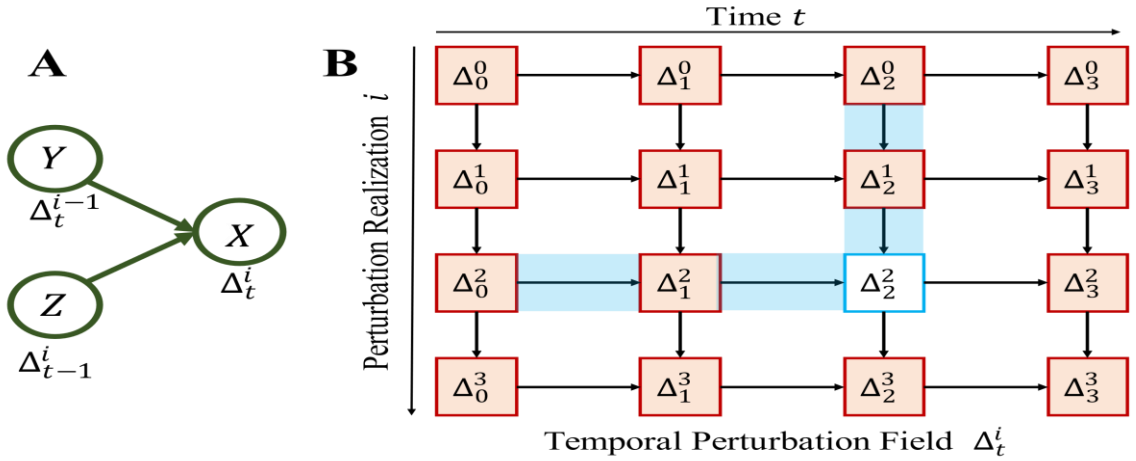


Figure 3. A. Graphical representation of the Bayesian Network. B. Perturbation Field viewed as a Bayesian Network. For any target value on the field (blue), there exists a forward pass and downward pass (shaded blue) to it.

**Results**

In this section, we give results of several experiments based on our approach described in previous section. We took cardiac activity data from ECG and analyzed it using our approach. Our principal objective was to compare Bayesian network parameters of Neural Temporal Perturbation Fields from normal and abnormal cardiac activity and devise new biomarkers. During optimization training of $\Theta$, we added Mean Squared Error (MSE) as regularization to the Log-likelihood function to find global maxima since usually MLE alone approximates to local maxima.

$$\mathcal{L}_{\text{MSE}} = \frac{1}{I \times T} \sum_{i \in I} \sum_{t \in T} \left\| \widehat{\Delta}_t^i - \Delta_t^i \right\|_2 \tag{9}$$

$$\Theta = \arg\max_{\Theta} \mathcal{L}(\Theta|X) \cap \arg\min \mathcal{L}_{\text{MSE}} \tag{10}$$

where $\Delta_t^i$ is the predicted value from the parameters in the log-likelihood step. From Figure 4-C, both forward and downward MSEs approaches zero as Log-Likelihood approaches local maxima. We also experimented with

Table 1. Optimized Parameters for Normal and Abnormal Cardiac Activity

| | Parameters | | | |
|---|---|---|---|---|
| | $C_f$ | $\sigma_f$ | $C_d$ | $\sigma_d$ |
| Normal | -0.21 | 3.67 | -0.23 | 3.63 |
| Abnormal | 1.20 | 5.91 | 1.37 | 6.01 |

the $AR$ order and discovered that, while it affects the initial MSE, the convergence time remains the same for both forward and downward passes (see Figure 4-D). Optimized weights $\Phi_f$ and $\Phi_d$ from normal and abnormal cardiac activity are shown in Figure 4-A. In normal activity, short range dependencies of order 2 $AR$ process ($\phi^0 + \phi^1$) is mostly excitatory (positive weights) while in abnormal activity, mostly inhibitory. In the case of long- range dependencies, the opposite case is observed. The parameters $\sigma_f$ and $\sigma_d$ represent volatility of the Neural Perturbation Field. From Figure 4-B, it is seen that optimum value of parameters maximizes the likelihood. Table 1 shows that the bias and volatility of both forward and downward passes are higher in abnormal activity than in normal activity.

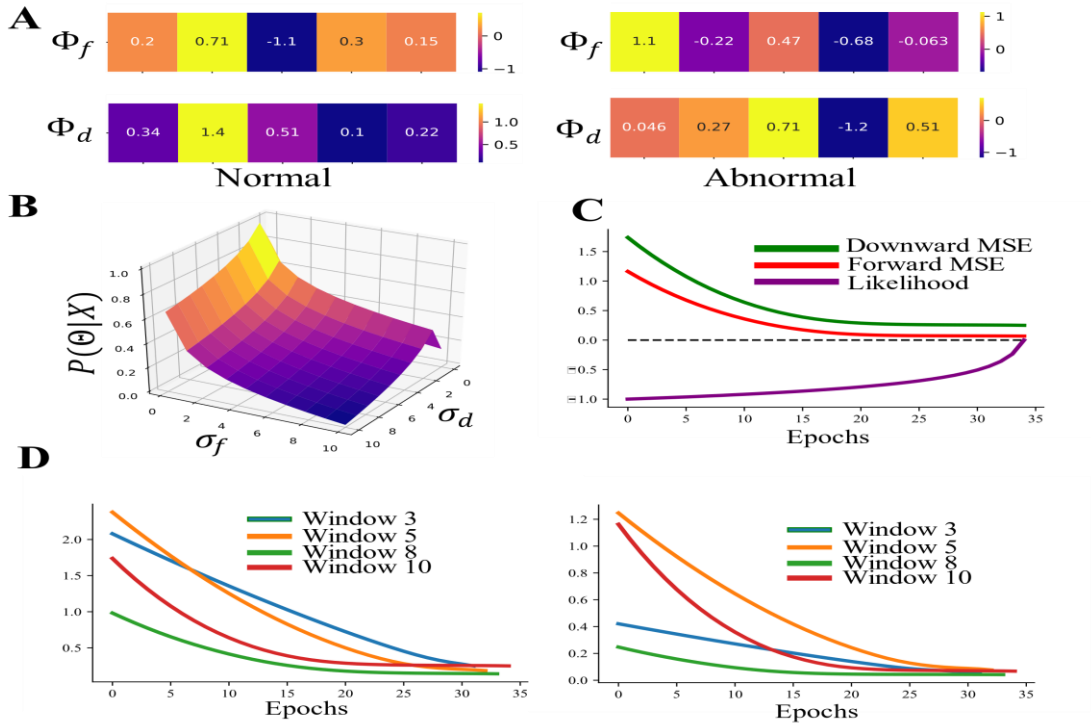


Figure 4. A. Weight vectors of forward and downward passes for normal and abnormal cardiac activity. B. Optimization graph of Log-likelihood graph for volatility parameters $\sigma_f$ and $\sigma_d$ for forward and downward passes respectively. C. MSE for forward and downward passes and Log-likelihood for the whole model. D. Effect of $AR$ order on MSE of forward (left) and downward passes (right).

## Conclusion

In this work, we have proposed a novel approach of studying cardiac activity through the lens of Perturbation Fields and Bayesian Networks. We found that our approach clearly explains the differences between regular and irregular cardiac activity through volatility, long-range and short-range dependencies in auto-regressive models. While previous approaches used Bayesian Networks as a mode of classification, we used that class of models to infer conclusions about the system from data. The advantage of our approach is that it can be applied to various kinds of biological and synthetic multi-variable time series data to draw conclusions form. In future works, we intend to explain brain activity using this approach while applying expertly selected priors to make the model more robust.

## References

Chugh, S. S., Reinier, K., Teodorescu, C., Evanado, A., Kehr, E., Al Samara, M., Mariani, R., Gunson, K., & Jui, J. (2008). Epidemiology of Sudden Cardiac Death: Clinical and Research Implications. *Progress in Cardiovascular Diseases*, *51*(*3*), 213–228. https://doi.org/10.1016/j.pcad.2008.06.003

Noponen, K., Kortelainen, J., & Seppänen, T. (2009). Invariant trajectory classification of dynamical systems with a case study on ECG. In *Pattern Recognition*, *42*(*9*), 1832–1844. https://doi.org/10.1016/j.patcog.2008.12.008

Shiogai, Y., Stefanovska, A., & McClintock, P. V. E. (2010). Nonlinear dynamics of cardiovascular ageing. In *Physics Reports*, *488*(*2–3*), 51–110. https://doi.org/10.1016/j.physrep.2009.12.003

Oliveira, D. L. S. C., Andreao, R. V., & Sarcinelli-Filho, M. (2011). Premature Ventricular beat classification using a dynamic Bayesian Network. *In 2011 Annual International Conference of the IEEE Engineering in Medicine and Biology Society*. 2011 33rd Annual International Conference of the IEEE Engineering in Medicine and Biology Society. IEEE. https://doi.org/10.1109/iembs.2011.6091235

Akhbari, M., Shamsollahi, M. B., & Jutten, C. (2017). Comparison of ECG fiducial point extraction methods based on dynamic Bayesian network. *In 2017 Iranian Conference on Electrical Engineering (ICEE)*. 2017 Iranian Conference on Electrical Engineering (ICEE). https://doi.org/10.1109/iraniancee.2017.7985197

Bousseljot R., Kreiseler D., Schnabel, A., Nutzung, D. E. K. G. Signaldatenbank, Cardiodat, D. P. T. B., Das, ü. (1995). Internet. *Biomedizinische Technik*, Band 40, Ergänzungsband 1, S 317.

Goldberger, A., Amaral, L., Glass, L., Hausdorff, J., Ivanov, P. C., Mark, R., & Stanley, H. E. (2000). PhysioBank, PhysioToolkit, and PhysioNet: Components of a new research resource for complex physiologic signals. *Circulation* [Online]. *101*(*23*), e215–e220.

Xie, Y., Takikawa, T., Saito, S., Litany, O., Yan, S., Khan, N., Tombari, F., Tompkin, J., Sitzmann, V., & Sridhar, S. (2021). Neural Fields in Visual Computing and Beyond (Version 4). *arXiv*. https://doi.org/10.48550/ARXIV.2111.11426

Balda, E. R., Behboodi, A., & Mathar, R. (2018). Perturbation Analysis of Learning Algorithms: A Unifying Perspective on Generation of Adversarial Examples (Version 1). *arXiv*. https://doi.org/10.48550/ARXIV.1812.07385

**Appendix A**

To get $P_{X|Y,Z}$, firstly, we need to define the following according to the Bayes theorem.

$$P_{X|Y,Z} = \frac{P_{X,Y,Z}}{P_{Y,Z}} \tag{11}$$

Now, from Figure 2-A, $P_{X,Y,Z}$ can be written as following.

$$P_{X,Y,Z} = P_{X,Y} P_{X,Z} \tag{12}$$

Using Equation 13 and 14, we get

$$P_{X|Y,Z} = \frac{P_{X,Y} P_{X,Z}}{P_{Y,Z}} = \frac{P_{X|Y} P_Y P_{X|Z} P_Z}{P_{Y,Z}} \tag{13}$$

$P_Y$ and $P_Z$ are independent of each other and therefore, $P_{Y,Z} = P_Y P_Z$.

$$P_{X|Y,Z} = P_{X|Y} P_{X|Z} \tag{14}$$

**Appendix B**

The log-likelihood function $\mathcal{L}(\Theta)$ can be detailed as follows.

$$\begin{aligned} \mathcal{L}(\Theta|\mathrm{X}) &= \log \prod_{i=w}^{|I|} \prod_{t=w}^{|T|} P_{X|Y}\left(\Delta_t^i\right) P_{X|Z}\left(\Delta_t^i\right) \\ &= \sum_{i=w}^{|I|} \sum_{t=w}^{|T|} \log\left[P_{X|Y}\left(\Delta_t^i\right) P_{X|Z}\left(\Delta_t^i\right)\right] \\ &= \sum_{i=w}^{|I|} \sum_{t=w}^{|T|} \left[\log P_{X|Y}\left(\Delta_t^i\right) + \log P_{X|Z}\left(\Delta_t^i\right)\right] \end{aligned} \tag{15}$$